# A Compliant, Underactuated Finger for Anthropomorphic Hands

George P. Kontoudis [1], Minas Liarokapis [2], and Kyriakos G. Vamvoudakis [3]

*Abstract*—This paper presents a compliant, underactuated finger for the development of anthropomorphic robotic and prosthetic hands. The finger achieves both flexion/extension and adduction/abduction on the metacarpophalangeal joint, by using two actuators. The design employs moment arm pulleys to drive the tendon laterally and amplify the abduction motion, while also maintaining the flexion motion. Particular emphasis has been given to the analysis of the mechanism. The proposed finger has been fabricated with the hybrid deposition manufacturing technique and the actuation mechanism's efficiency has been validated with experiments that include the computation of the reachable workspace, the assessment of the exerted forces at the fingertip, the demonstration of the feasible motions, and the presentation of the grasping and manipulation capabilities. The proposed mechanism facilitates the collaboration of the two actuators to increase the exerted finger forces. Moreover, the extended workspace allows the execution of dexterous manipulation tasks.

## I. INTRODUCTION

The human hand is considered to be Nature's most dexterous end-effector and the goal of replicating human dexterity has motivated roboticists to follow bio-inspired approaches [1]–[4]. One of the most important joints in the human hand is the metacarpophalangeal joint (MCP), which allows the fingers to execute both adduction/abduction and flexion/extension motions, thus increasing the dexterity of the overall system. In addition, it has been shown that the execution of the abduction on the MCP joint enhances the grasping capabilities of robot hands. More specifically, the abduction is the dominant motion of the second principal component that augments the grasping capabilities by 17%, as reported in [5]. Moreover, the human thumb's MCP joint is responsible for the opposition which is a significant motion of the human hand [6], [7]. The focus of this work is on enhancing the robotic finger's performance, facilitating the execution of various grasping and in-hand manipulation tasks in a simplified manner, without compromising dexterity [8].

In [9], the authors proposed a double active universal joint that was implemented with gear transmission and two actuators. Xu et al. [10] introduced an anthropomorphic robotic finger with pin joints that employed biomimetic crocheted ligaments and tendon-routing system. Their objective was to develop a robotic finger that has identical function with the human fingers. In [11], the authors proposed a compliant robotic finger design that integrates passive parallel compliance. Their design combines elastomer materials along with a specific structure that performs as a variable stiffness compliant joint towards improving the stability of the system in grasping and manipulation. These fingers are considered adaptive, since they are underactuated and equipped with flexure or spring loaded pin joints. The flexion/extension analysis for robotic fingers with pin joints and flexure joints has been studied in [12], [13], and [14] respectively. In [15] an analytical modeling of flexure joints based on screw theory was presented. In addition, the authors fabricated a gripper to demonstrate its grasping capabilities. A soft monolithic finger was presented in [16]. The authors investigated various types of flexure joints and fabricated a robotic finger. Yet, the adduction/abduction motion was not studied. In [17], the authors presented a rotational elastic joint for underactuated robotic fingers. Their design is monolithic and the joint is implemented with an embedded spiral torsional spring. Regarding anthropomorphism of robot motion, a previous study [18] investigated the affinity in structure and motion of robotic hands and the human hand. This study proposed a methodology for the quantification of robot hands anthropomorphism that combined computational geometry and set theory methods for advanced human and robot hand workspace comparisons, providing a score of humanlikeness.

The main contribution of this paper is a compliant, underactuated finger with improved dexterity. The actuation mechanism design is minimal and modular, as it makes use of simple mechanical elements. The fingers used are adaptive, consisting of flexure joints based on elastomer materials. The proposed mechanism has the ability to perform concurrently flexion/extension and adduction/abduction on the MCP joint, by employing two actuators. Appropriate design parameters are provided for the execution of various adduction/abduction motions through a mechanism analysis. The ability of the actuation mechanism to increase the force exertion capabilities of the finger has been demonstrated. The grasping and manipulation capabilities have been experimentally validated. The proposed finger can be used for the development of adaptive robotic and prosthetic hands.

The remainder of this paper is organized as follows. Section II focuses on the design of the actuation mechanism and performs an analysis of the design constraints, Section III, we present the developed finger, Section IV provides the experimental validation, while Section V concludes the paper and discusses future directions.

[1]George P. Kontoudis is with the Kevin T. Crofton Department of Aerospace and Ocean Engineering, Virginia Tech, Blacksburg, VA 24060, USA, email: gpkont@vt.edu.

[2]Minas Liarokapis is with the New Dexterity research group, Department of Mechanical Engineering, University of Auckland, Auckland, 1010, New Zealand, email: minas.liarokapis@auckland.ac.nz.

[3]Kyriakos G. Vamvoudakis is with the Daniel Guggenheim School of Aerospace Engineering, Georgia Tech, GA 30332, USA, USA, email: kyriakos@gatech.edu.
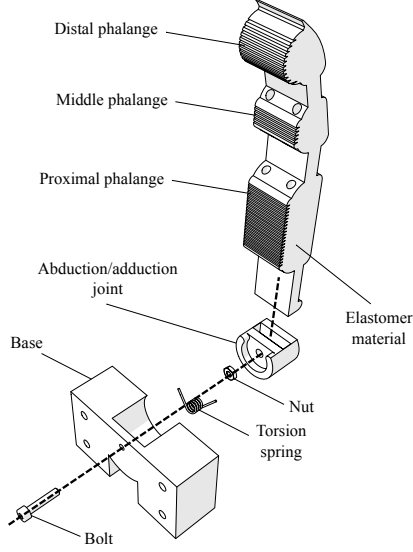
Fig. 1. An exploded view of the finger's 3D model. The finger structure is compliant as it combines an elastic body (urethane rubber) with plastic parts (e.g., tendon routing tubes and joint base). The design is also modular, as it is connected to the palm with a single bolt-nut set.
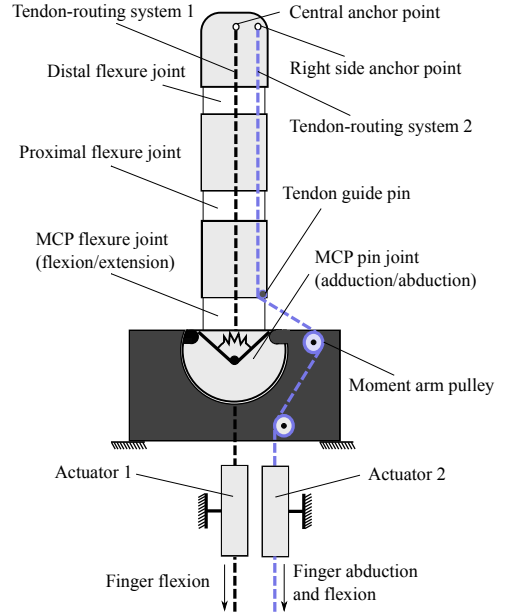


Fig. 2. The actuation mechanism that allows for flexion/extension and adduction/abduction concurrently is presented. The finger operates a clockwise motion. For counterclockwise motion, the right side anchor point needs to be swifted to the left side. For bidirectional abduction, the central anchor point needs to be placed on the left side of the finger.

## II. FINGER DESIGN AND ACTUATION MECHANISM

In this section, we present the design of the adaptive robot finger and we describe the tendon-driven actuation mechanism. The actuation mechanism analysis is provided to specify design parameters for various applications.

### A. Actuation Mechanism Design

The finger structure is monolithic and consists of an elastic body (made out of urethane rubber) and plastic parts, as presented in Fig. 1. The robotic finger is actuated by artificial tendons. The distal, middle, and proximal phalanges as well as the flexure joints (areas of reduced thickness) are implemented with an elastomer material. The MCP spring loaded pin joint is responsible for the adduction/abduction. The design is also modular since the fingers are attached in the base frame with a single bolt-nut set.

The actuation mechanism utilizes two independent tendon-routing systems to actuate the finger, as shown in Fig. 2. We equip the proposed actuation mechanism with moment arm pulleys to drive the tendon-routing system through a specific path, that is illustrated with a dashed blue line. On this path, the line of action of the applied force is increased. Therefore, the forces transferred through the tendon-routing system, create a moment that rotates the finger. Each tendon is responsible for a different motion. The tendon with ending point at the central anchor (connected with the first actuator) is only responsible for the flexion/extension motion of the finger. The tendon with ending point at the right side anchor point (connected with the second actuator) triggers initially the adduction/abduction motion and then contributes to the flexion/extension of the finger. This twofold contribution in motion and force transmission lies in the design choice to

place the right side anchor point at the distal phalange and not to the middle or the proximal phalange. In case of concurrent actuation of both motors the flexion/extension is the dominant motion.

The selection of anchor points for each separate tendon-routing system is determined according to the desired finger motion. One can notice that from the human hand neutral position, the index abduction moves oppositely from the ring and pinky abduction motions. The abduction motion from the natural position of the middle finger can be neglected, since it is relatively small. On the other hand, the thumb motion includes bidirectional adduction/abduction. Therefore, for an anthropomorphic hand design we should be able to produce three different types of finger abductions. For this purpose, we employ right-side anchor points for clockwise motion, left-side anchor points for counterclockwise motion, and both-sides anchor points for bidirectional rotation. In case we pursue single side rotation, central anchor points utilization is needed to impose the finger flexion/extension movements.

### B. Actuation Mechanism Analysis

Since our focus is on the adduction/abduction motion, we need to determine the corresponding design characteristics. For our analysis we consider that the stiffness of the flexure joints is much larger than the stiffness of the torsion spring $k_\mathrm{d}, k_\mathrm{p}, k_\mathrm{fm} \gg k_\mathrm{t}$. The stiffness of the flexure joints affects the forces that can be transmitted to the finger, so the flexure joint stiffness $k_\mathrm{d}, k_\mathrm{p}, k_\mathrm{fm}$ need to be high. On the other hand, the torsion spring $k_\mathrm{t}$ needs to be stiff enough to compensate gravity and successfully rebound the finger to its rest position.
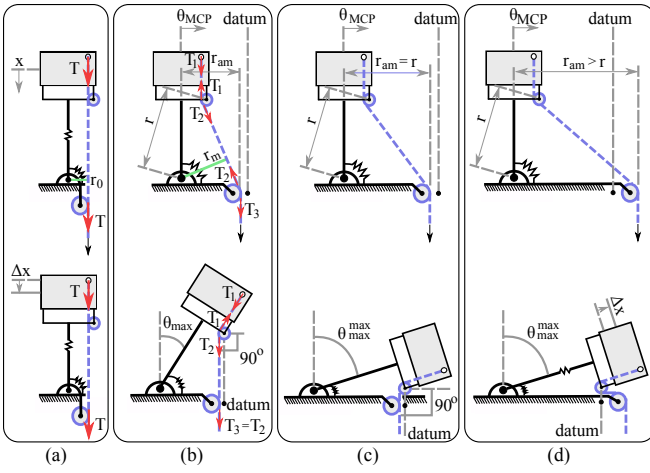
Fig. 3. The actuation mechanism in various configurations. Different design choices with respect to the moment arm pulley position, produce various abduction motions. (a) The moment arm pulley is perpendicular to the tendon guide pin. (b) The moment arm pulley is in an intermediate position. (c) The distance from the joint axis of rotation to the moment arm pulley $r_{am}$ matches the radius length $r$. (d) The distance from the joint axis to the moment arm pulley $r_{am}$, is higher than the radius length $r$.
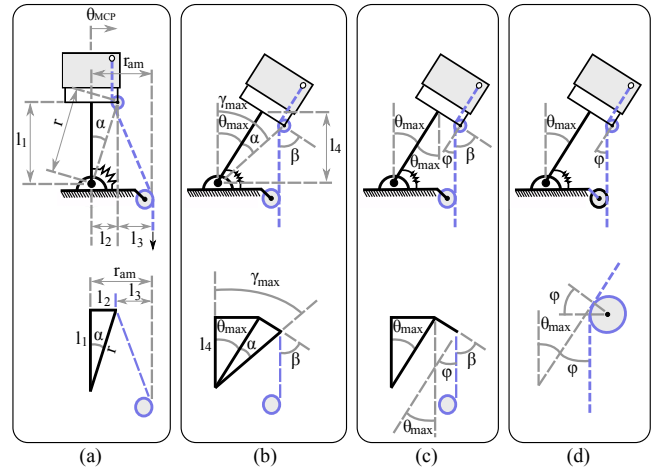


Fig. 4. The actuation mechanism model at the initial and at the maximum abduction configuration. The Subfigures present the mechanism character-istics at: (a) the initial configuration, (b, c) the maximum abduction angle, (d) the tendon guide pin for a maximum abduction angle.

The key idea underlying the actuation mechanism is that by selecting various moment arm pulley positions we will be able to achieve different maximum abduction angles as presented in Fig. 3. The maximum abduction angle occurs when the moment arm is eliminated. Therefore, the actuator that is responsible for the adduction/abduction first triggers the abduction, until it reaches its higher possible abduction angle, and then contributes to the flexion/extension motion as depicted in the lower part of Fig. 3. When the moment arm pulley is by design perpendicular with the tendon guide pin, then the mechanism will trigger only perpendicular motion $\Delta x$, as the line of action of the resultant forces will pass through the center of the pulley's axis of rotation as shown in Subfig. 3(a). In case that we select the position of the moment arm pulley at a horizontal distance $r_{am}$, then the mechanism will be abducted until the line of action becomes collinear with the pulley's axis of rotation at $\theta_{max}$, as depicted in Subfig. 3(b). Next, for the maximum abduction angle $\theta_{max}^{max}$ the moment arm pulley should be placed at a distance $r_{am} = r$ as presented in Subfig. 3(c). The last possible choice is to place the moment arm pulley at a distance $r_{am} > r$ where the finger will first reach its maximum abduction $\theta_{max}^{max}$, but then it will be subject to tensile stress with a $\Delta x$ deformation as shown in Subfig. 3(d). Note that the moment arm in Subfig. 3(a) is relatively small so that the torsional spring and the friction eliminate its effect.

Our goal is to specify the design parameters in order to achieve the desired abduction angle $\theta_{max}$ in the mechanism. For the adduction/abduction motion analysis, the actuation mechanism model is depicted in Fig. 4. The $l_1$ is the joint length and the $l_2$ is the moment arm distance, which is imposed by the initial position of the tendon guide pin and the moment arm pulley. The actuation mechanism has an internal angle $\alpha$ that is invariant of the actuator displacement

and depends only on the mechanism design. The mechanism can achieve abduction angles $\theta_{MCP} \in [-\frac{\pi}{2} + \alpha, \frac{\pi}{2} - \alpha]$ for bidirectional abduction. Since our analysis deals with clockwise abduction, the mechanism achieves $\theta_{MCP} \in [0, \frac{\pi}{2} - \alpha]$. The angle $\beta$ is formed by the perpendicular line of the link and the tendon. The length $l_3$ is the distance from the tendon guide pin to the moment arm pulley. The distance from the abduction joint axis of rotation to the tendon guide pin is illustrated by $r$. As the mechanism performs abduction the distance $r_{am}$ remains constant. On the other hand, the perpendicular distance from the abduction joint axis to the guide pin decreases to $l_4$, when the mechanism arrives at its maximum abduction angle.

The variable that imposes the moment arm is also respon-sible for the maximum abduction angle. That is, the length $l_3$ at the initial configuration without any actuator displacement. Given the finger design characteristics $l_1$, $l_2$ and the desired maximum abduction angle $\theta_{max}$, we need to find the length $l_3$. At the maximum abduction angle we have $\theta_{max} = \gamma_{max} - \alpha$. Then, from the initial configuration we obtain,

$$\alpha = \arctan\left(\frac{l_2}{l_1}\right). \quad (1)$$

Next, we find the maximum abduction angle $\gamma_{max}$ as follows,

$$\sin\gamma_{max} = \sin(\theta_{max} + \alpha) = \frac{r_{am}}{r}. \quad (2)$$

Given that $r_{am} = l_2 + l_3$, the eq. (2) takes the form of,

$$l_3 = \sin(\theta_{max} + \alpha)r - l_2. \quad (3)$$

Considering that at the initial configuration the length $r = \sqrt{l_1^2 + l_2^2}$, we express the desired length $l_3$ exclusively as a function of the maximum abduction angle $\theta_{max}$ and the finger design characteristics $l_1$, $l_2$ from eq. (3) as follows,

$$l_3 = \sin\left[\theta_{max} + \arctan\left(\frac{l_2}{l_1}\right)\right]\left(\sqrt{l_1^2 + l_2^2}\right) - l_2. \quad (4)$$

## C. Smooth Curvature Model

In our design, most of the joints employ elastomer materials, i.e. they are flexure joints. To this end, the rotational stiffness of the MCP joint $k_{\text{fm}}$, of the PIP joint $k_{\text{p}}$, and of the DIP joint $k_{\text{d}}$ require further analysis. We employ the smooth curvature model and we provide here a brief description. A detailed analysis of flexure joint stiffness as well as a low-dimensional forward kinematic method, can be found in [14].

The smooth curvature model is an approximation of the Euler-Bernoulli large bending model and utilizes only three parameters. To determine the generalized stiffness matrix, we compute the Hessian of both the internal and external work as follows,

$$\mathbf{K}_{\text{flex}} = \nabla_\zeta^2 U - (\nabla_\zeta^2 x_{\text{tip}})P_{\text{x}} - (\nabla_\zeta^2 y_{\text{tip}})P_{\text{y}}, \quad (5)$$

where $\zeta = [\varphi \ x \ y]^\mathsf{T} \in \mathbb{R}^3$ is the vector of parameters for planar approximation, $U$ is the energy of the flexure, $x_{\text{tip}}$, $y_{\text{tip}}$ are the $x$, $y$ coordinates of the flexure tip respectively, and $P_{\text{x}}$, $P_{\text{y}}$ the applied load at the $x$, $y$ directions of the flexure tip respectively. Note that the Hessian of the angle at the flexure tip is eliminated. The energy term in (5) yields,

$$\nabla_\zeta^2 U = \frac{E_{\text{flex}}I_{\text{flex}}}{L_{\text{flex}}} \begin{bmatrix} 1 & 0 & 0 \\ 0 & 1/3 & 0 \\ 0 & 0 & 1/5 \end{bmatrix}, \quad (6)$$

where $E_{\text{flex}}$ is the Young's modulus, $I_{\text{flex}}$ is the moment of inertia, and $L_{\text{flex}}$ is the length of the flexure joint. The Young's modulus is assumed to be constant, similarly to [19]. Also, the moment of inertia of a rectangular area is, $I_{\text{flex}} = \frac{bh^3}{12}$, where $b$ is the flexure width and $h$ is the flexure thickness.

We consider that the flexure joint is subject to large load and buckling. We account for buckling by employing the Euler's critical load equation,

$$P_{\text{cr}} = \frac{\pi^2 E_{\text{flex}}I_{\text{flex}}}{4L_{\text{flex}}^2}. \quad (7)$$

Therefore, without any boundary conditions at the flexure tip, i.e. free tip, the (5) from (6) and (7) results to the symmetric global stiffness matrix as,

$$\mathbf{K}_{\text{flex}} = \nabla_\zeta^2 U + LP_{\text{cr}} \begin{bmatrix} -1/3 & 1/12 & 1/60 \\ 1/12 & -1/30 & 0 \\ 1/60 & 0 & -1/210 \end{bmatrix}$$

$$= \frac{E_{\text{flex}}I_{\text{flex}}}{L_{\text{flex}}} \begin{bmatrix} \frac{12-\pi^2}{12} & \frac{1}{12} & \frac{1}{60} \\ \frac{1}{12} & \frac{360-\pi^2}{360} & 0 \\ \frac{1}{60} & 0 & \frac{4200-\pi^2}{4200} \end{bmatrix}. \quad (8)$$

Next, we seek to associate the rotational flexure stiffness $k_{\text{flex}}^{\text{rot}} = k_{\text{fm}} = k_{\text{p}} = k_{\text{d}}$ to the global stiffness matrix $\mathbf{K}_{\text{flex}}$. Without loss of generality we assume straight curvature $\kappa = 0$ when then flexure joint is flexed in the free space, [20]. In Fig. 5, we present a flexure joint with similar performance to the proposed adaptive finger joints. One side of the joint is fixed to the inertial frame $\mathcal{F}_{\text{a}}$ and the other side performs a planar free motion with a body-fixed frame $\mathcal{F}_{\text{b}}$ at the flexure tip. It is easy to see that the flexure joint configuration
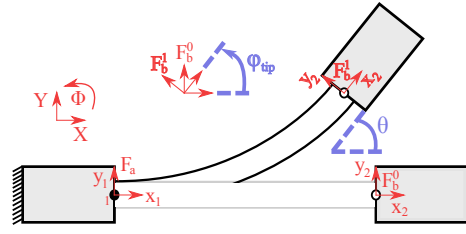


Fig. 5. A flexure joint with straight curvature, $\kappa = 0$. One link is fixed at inertial frame $\mathcal{F}_{\text{a}}$ while the other link performs a planar motion with a body-fixed frame $\mathcal{F}_{\text{b}}$. The flexure tip angle $\varphi_{\text{tip}}$, described by the rotation of body-fixed frame $\mathcal{F}_{\text{b}}$, is equal with the joint angle $\theta$.

matches with the flexure tip rotation, i.e. $\theta = \varphi_{\text{tip}}$. Thus, the rotational flexure stiffness under large load and buckling yields,

$$k_{\text{flex}}^{\text{rot}} = \begin{bmatrix} 1 & 0 & 0 \end{bmatrix} \mathbf{K}_{\text{flex}} \begin{bmatrix} 1 \\ 0 \\ 0 \end{bmatrix} = \frac{12-\pi^2}{12} \frac{E_{\text{flex}}I_{\text{flex}}}{L_{\text{flex}}}$$

$$= 0.1775 \frac{E_{\text{flex}}I_{\text{flex}}}{L_{\text{flex}}}. \quad (9)$$

In case that the flexure joint is only subject to large load, the smooth curvature model results to rotational flexure stiffness of $k_{\text{flex}}^{\text{rot}} = \frac{E_{\text{flex}}I_{\text{flex}}}{L_{\text{flex}}}$, as in [21]. However, in realistic scenarios the flexure joints will be subject to buckling. To this end, the rotational flexure stiffness is required to be almost five times larger to account for buckling. Note also that the effect of the flexure joint thickness $h$ to the realized stiffness $k_{\text{flex}}^{\text{rot}}$ is proportional to its power of three.

## III. Developed Finger

We derive appropriate dimensions of the adaptive robot finger based on anthropometric data [22]. Since the finger length and the finger breadth are predetermined, the only parameter that we can select to achieve different rotational flexure stiffness values, is the flexure joint thickness $h$. The design parameters that affect the finger's motion are the moment arm pulley position, the elastomer material stiffness of the flexure joints, and the torsional spring stiffness. The ideal bending profile of the finger — that depends on the stiffness ratio of the flexure joints — is selected using the anthropomorphism index, proposed by [18], and the maximum desired flexion angle range [6]. The polyurethane rubber material specifications are provided by the manufacturer (Smooth-On - PMC 780). The anthropomorphic parameters were computed for hand length HL= 185 mm and hand breadth HB= 90 mm, as discussed in [23].

Next, we compute the radius of the moment arm pulley for a desired abduction. According to our analysis in Sub-section II-B, for maximum abduction angle $\theta_{\text{max}} = 67.5^\circ$, MCP flexure joint length $L_{\text{flex,m}} = l_1 = 7.00$ mm, and tendon distance $l_2 = 5.10$ mm, the required distance from the abduction joint axis to the moment arm pulley from (4) results to $r_{\text{am}} = 8.42$ mm, as presented in Table I. We assumed non-anthropomorphic, extreme abduction angle range to demonstrate the efficacy of the actuation mechanism.

TABLE I

MCP JOINT CHARACTERISTICS FOR ABDUCTION

| Description | Parameter | Value |
|---|---|---|
| Desired Max. Abduction | $\theta_{\max}$ [deg] | 67.50 |
| Tendon Distance | $l_2$ [mm] | 5.10 |
| Length | $L_{\text{flex,m}} = l_1$ [mm] | 7.00 |
| Computed Radius | $r_{\text{am}}$ [mm] | 8.42 |



Fig. 6. The fabrication porcess of the developed finger. (a) The reusable mold in blue, the rotating base in purple, and the sacrificial mold in black. (b) The elastomer material at the curing phase. (c) Side views and front view of the fabricated finger.

Moreover, we want to validate our analysis by conducting kinematic experiments with the fabricated finger. We show in Subsection IV-A that the finger achieves the desired maximum abduction angle of 67.5º. Next, we compute the rotational flexure stiffness of the MCP joint $k_{\text{fm}}$, of the PIP joint $k_{\text{p}}$ and of the DIP joint $k_{\text{d}}$. We consider flexure joint thickness $h_{\text{fm}} = 5.00$ mm and flexure joint length $L_{\text{flex,m}} = l_1 = 7.00$ mm. The resulted stiffness values are computed by (9) and they are presented in Table II.

TABLE II

ROTATIONAL JOINT STIFFNESS AND TENDON FORCE

| Joints | Thickness [mm] | Stiffness [N.m/rad] |
|---|---|---|
| DIP F/E | $h_{\text{d}} = 6.00$ | $k_{\text{d}} = 0.0235$ |
| PIP F/E | $h_{\text{p}} = 6.00$ | $k_{\text{p}} = 0.0235$ |
| MCP F/E | $h_{\text{fm}} = 5.00$ | $k_{\text{fm}} = 0.0120$ |
| MCP A/A | - | $k_{\text{t}} = 0.0105$ |

We have used exclusively off-the-shelf materials that reduce the cost and expedite the fabrication process. The fabrication procedure and the adaptive finger are presented in Fig. 6. We employed the Hybrid Deposition Manufacturing (HDM) technique [24] using two different molds. More specifically, we use a reusable mold (blue), a rotating base (purple), and a sacrificial mold (black), as presented in Subfig. 6(a). The sacrificial mold has holes to penetrate the low friction tubes (green parts), as shown in Subfig. 6(b). Then, the reusable mold accommodates the sacrificial mold and the rotating base to prevent elastomer leakage, as depicted in Subfig. 6(c).

Regarding actuation, we equip the robotic finger with 2 Dynamixel RX-28 servo motors with torque $T_{\text{m}} = 2.8$ Nm at 12V and outer shaft diameter $D_{\text{m}} = 2.50$ mm for the flexion/extension and adduction/abduction. Then, we place a pulley to the outer shaft with diameter $D_{\text{p}} = 50.00$ mm. The resulting tendon force of each actuator is $f_{\text{a}} = 112$ N. Note that we use motors with significantly higher torque to guarantee robustness of grasping.

## IV. RESULTS AND EXPERIMENTS

In this section, we evaluate the efficiency of the actuation mechanism. First, we compute the workspace of the robotic finger. Then, we analyze the grasping forces to investigate the force exertion capabilities of the finger and we assure that the joint preserves its position when it is abducted. We also perform a force comparison with a finger at the
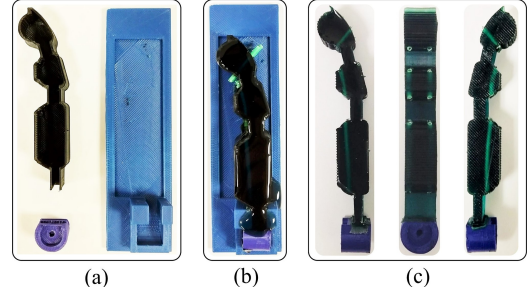
fully abducted position. Furthermore, we validate the efficacy of the proposed finger design by performing two set of experiments that include the implementation of various finger postures and the manipulation of an object.

### A. Finger Workspace

We employed a standard Kinect camera (Microsoft) with 3 markers at the center of each flexure joint, 1 marker at the MCP axis of rotation for the abduction, and 1 marker at the edge of the fingertip. Then we build the workspace by connecting the 3D points and computing the convex hulls. In Fig. 7, the finger workspace with one side rotation is presented. The maximum angle that was attained by the MCP joint is 67.5º, thus our analysis is valid. All the intermediate configurations can be achieved by combing the 2 actuators. Also, the top view in Subfig. 7(b) depicts the coupling between the flexion and the abduction at the extreme abduction angle.

The proposed actuation mechanism is amplifying the workspace, comparing to finger designs that accomplish only flexion/extension. This workspace extension will allow for the execution of dexterous manipulation tasks.

### B. Force Exertion Capabilities

We gather the fingertip exerted forces in various configurations of a single digit. To do so, we employed the FSE1001 force sensor (Variense). Next, we measure repeatedly the exerted forces that occurred for only flexion by employing both actuators. Similarly, we measure the fingertip forces in fully abducted configuration by employing again both actuators. The experimental procedure is adopted from the finger strength measure protocol proposed by [25]. That is a kinetic measure of the maximum force that a robotic finger can impose on its environment. In addition, we evaluated the force exertion capabilities during abduction.

We acquire the finger forces from 20 trials. The comparison of the fingertip exerted forces in two configurations is shown in Fig. 8. The overall mean exerted forces are illustrated on the right side with dashed line. The solid line represents the mean value at each time step, while the shadowed area depicts the standard deviation. The black-gray colored area depicts the finger forces during only flexion and

Fig. 8. A comparison of the fingertip exerted forces in two different configurations. The performance of the finger is quite similar at every trial. The finger exerts similar forces even at the fully abducted position. The momentum of the finger during contact produces the overshoot.
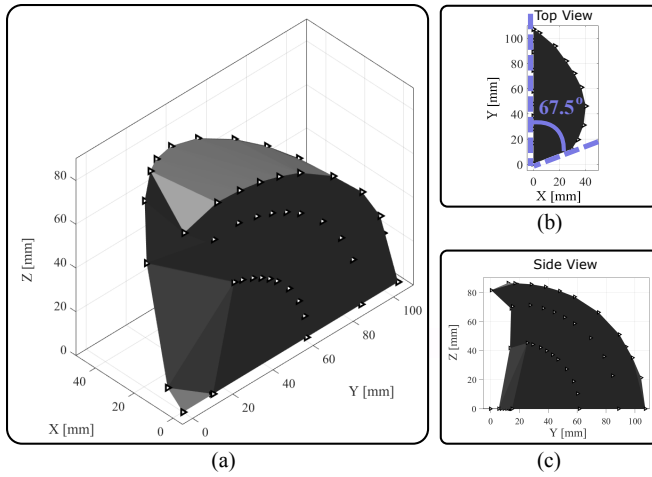
Fig. 7. The reachable workspace of an anthropomorphic index finger. The triangular points represent the position of the joints through time. (a) Perspective view. (b) The top view illustrates the finger abduction. (c) The side view depicts the finger flexion.

the blue-light colored area the finger forces during flexion in fully abducted position. The reported overall mean value for only flexion (for the quasi-static case, i.e. by ignoring the dynamic contact forces) is 11.1 N. The standard deviation reveals that the performance of the finger is similar at every trial. The actuation mechanism not only maintains its position from the maximum abducted configuration while flexed, but it also reports a force of 9.3 N. As the finger is abducted, the achievable finger force is reduced, because of various friction losses, yet the force exertion remains significantly high.

## C. Grasping and Manipulation Capabilities

First, we perform finger posture experiments that include an individual finger flexion, an individual finger abduction, a finger flexion at the highest abduction configuration, and a finger abduction at the highest flexion configuration. The finger configurations of flexion and abduction are presented in Fig. 9. We are able to replicate the adduction/abduction capabilities of all human hand fingers. More specifically, for a left hand, from the palm side view, it is required, counterclockwise motion for the index, clockwise motion for the ring and pinky, and bidirectional motion for the thumb.

Next, we conduct grasping and manipulation experiments with a cylindrical object. The object was fabricated with 3D printed ABS material, it has a diameter $D = 25$ mm, and length $h = 50$ mm. The grasping and manipulation experiments are depicted in Fig. 10. First, the finger and a fixed surface are used to perform a robust grasping action. Then, the finger rolls the object bidirectionally from $0°$ to $-45°$, from $-45°$ to $45°$, and from $-45°$ to $0°$. The rolling did not cause any object slip as it successfully returns at its initial position, which is indicated by a black mark on the object. This experiment reveals the grasping and manipulation capabilities of the proposed single bidirectional adaptive finger.
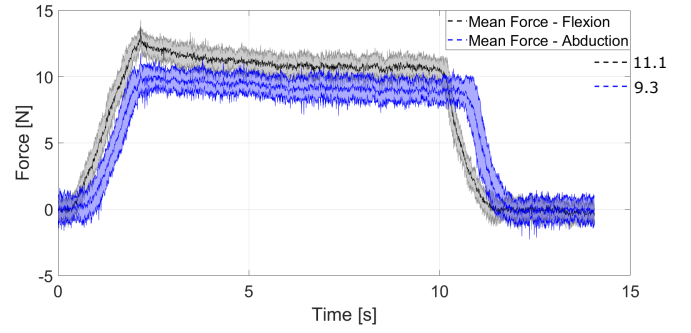
## V. Conclusions and Future Work

This paper proposed an anthropomorphic finger equipped with a novel actuation mechanism. The finger is capable of implementing concurrently flexion/extension and adduction/abduction. We presented the joint's specifications and we performed a mechanism analysis that derives the appropriate parameters for the implementation of various abduction configurations. A flexure model was discussed that derives the stiffness value of each flexure joint. The exerted force results show a force range between 9.3 N to 11.1 N for the two extreme conditions. Moreover, the workspace has increased significantly, indicating an enhancement in the overall system dexterity. Next, we validated the actuation mechanism's performance by providing experimental paradigms conducted with an anthropomorphic, adaptive robot finger and a fixed surface. The finger achieves both adduction/abduction and flexion/extension, resulting to various configurations. The finger is able to execute both robust grasping and dexterous manipulation tasks without any slip.

The proposed actuation mechanism will render adaptive robotic and prosthetic hands even more human-like and dexterous. Ongoing work is focusing on the design and development of a complete anthropomorphic hand employing the proposed actuation mechanism. The idea is to utilize differential mechanisms to perform flexion/extension and adduction/abduction of four fingers by employing only two actuators.

### References

[1] S. A. Dalley, T. E. Wiste, T. J. Withrow, and M. Goldfarb, "Design of a multifunctional anthropomorphic prosthetic hand with extrinsic actuation," *IEEE/ASME Transactions on Mechatronics*, vol. 14, no. 6, pp. 699–706, 2009.

[2] A. D. Deshpande, Z. Xu, M. J. V. Weghe, B. H. Brown, J. Ko, L. Y. Chang, D. D. Wilkinson, S. M. Bidic, and Y. Matsuoka, "Mechanisms of the anatomically correct testbed hand," *IEEE/ASME Transactions on Mechatronics*, vol. 18, no. 1, pp. 238–250, 2013.

[3] C.-H. Xiong, W.-R. Chen, B.-Y. Sun, M.-J. Liu, S.-G. Yue, and W.-B. Chen, "Design and implementation of an anthropomorphic hand for replicating human grasping functions," *IEEE Transactions on Robotics*, vol. 32, no. 3, pp. 652–671, 2016.

[4] Z. Xu and E. Todorov, "Design of a highly biomimetic anthropomorphic robotic hand towards artificial limb regeneration," in *IEEE International Conference on Robotics and Automation*, 2016, pp. 3485–3492.
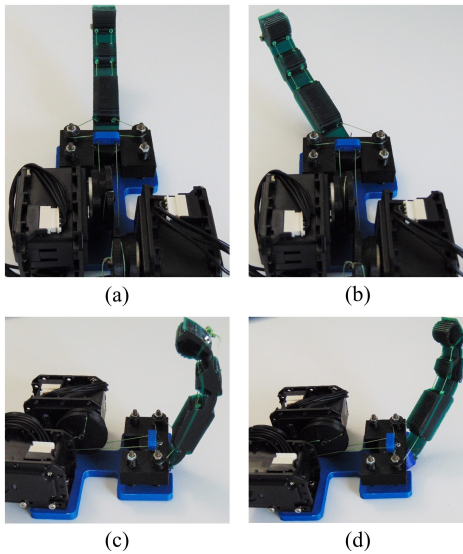
Fig. 9. The anthropomorphic finger in various configurations. (a) Finger in the neutral (rest) position. (b) Finger abduction achieved by using the corresponding tendon-driven system. (c) Finger flexion without any abduction. (d) Finger flexion in an abducted angle.
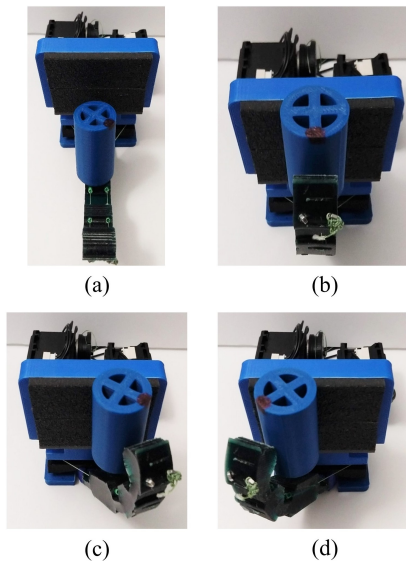


Fig. 10. The anthropomorphic finger performing a manipulation task. (a) The adaptive finger with the cylindrical object. (b) Initial grasping position. (c) Rolling clockwise $45°$. (d) Rolling counterclockwise $90°$.

[5] M. Santello, M. Flanders, and J. F. Soechting, "Postural hand synergies for tool use," *Journal of Neuroscience*, vol. 18, no. 23, pp. 10 105–10 115, 1998.

[6] I. Kapandji, *Physiology of the joints: Upper limb*, 6th ed. Churchill Livingstone Edinburgh, 1974, vol. 1.

[7] V. K. Nanayakkara, G. Cotugno, N. Vitzilaios, D. Venetsanos, T. Nanayakkara, and M. N. Sahinkaya, "The role of morphology of the thumb in anthropomorphic grasping: a review," *Frontiers in Mechanical Engineering*, vol. 3, p. 5, 2017.

[8] A. Bicchi, "Hands for dexterous manipulation and robust grasping: A difficult road toward simplicity," *IEEE Transactions on Robotics and Automation*, vol. 16, no. 6, pp. 652–662, 2000.

[9] S. Ryew and H. Choi, "Double active universal joint (DAUJ): Robotic joint mechanism for human-like motions," *IEEE Transactions on Robotics and Automation*, vol. 17, no. 3, pp. 290–300, 2001.

[10] Z. Xu, V. Kumar, Y. Matsuoka, and E. Todorov, "Design of an anthropomorphic robotic finger system with biomimetic artificial joints," in *IEEE-RAS/EMBS International Conference on Biomedical Robotics and Biomechatronics*, 2012, pp. 568–574.

[11] P.-H. Kuo and A. D. Deshpande, "A novel joint design for robotic hands with humanlike nonlinear compliance," *Journal of Mechanisms and Robotics*, vol. 8, no. 2, pp. 021 004 1–10, 2016.

[12] L. Birglen and C. M. Gosselin, "Kinetostatic analysis of underactuated fingers," *IEEE Transactions on Robotics and Automation*, vol. 20, no. 2, pp. 211–221, 2004.

[13] T. D. Niehues, R. J. King, A. D. Deshpande, and S. Keller, "Development and validation of modeling framework for interconnected tendon networks in robotic and human fingers," in *IEEE International Conference on Robotics and Automation*, 2017, pp. 4181–4186.

[14] L. U. Odhner and A. M. Dollar, "The smooth curvature model: An efficient representation of Euler–Bernoulli flexures as robot joints," *IEEE Transactions on Robotics*, vol. 28, no. 4, pp. 761–772, 2012.

[15] I. Hussain, F. Renda, Z. Iqbal, M. Malvezzi, G. Salvietti, L. Seneviratne, D. Gan, and D. Prattichizzo, "Modeling and prototyping of an underactuated gripper exploiting joint compliance and modularity," *IEEE Robotics and Automation Letters*, vol. 3, no. 4, pp. 2854–2861, 2018.

[16] R. Mutlu, G. Alici, M. in het Panhuis, and G. M. Spinks, "3D printed flexure hinges for soft monolithic prosthetic fingers," *Soft Robotics*, vol. 3, no. 3, pp. 120–133, 2016.

[17] U. Scarcia, G. Berselli, G. Palli, and C. Melchiorri, "Modeling, design, and experimental evaluation of rotational elastic joints for underactuated robotic fingers," in *IEEE-RAS International Conference on Humanoid Robotics*, 2017, pp. 353–358.

[18] M. V. Liarokapis, P. K. Artemiadis, and K. J. Kyriakopoulos, "Quantifying anthropomorphism of robot hands," in *IEEE International Conference on Robotics and Automation*, 2013, pp. 2041–2046.

[19] H. S. Stuart, S. Wang, B. Gardineer, D. L. Christensen, D. M. Aukes, and M. Cutkosky, "A compliant underactuated hand with suction flow for underwater mobile manipulation," in *IEEE International Conference on Robotics and Automation*, 2014, pp. 6691–6697.

[20] J. Guo and K.-M. Lee, "Compliant joint design and flexure finger dynamic analysis using an equivalent pin model," *Mechanism and Machine Theory*, vol. 70, pp. 338–353, 2013.

[21] L. L. Howell, "Compliant mechanisms," in *Encyclopedia of Nanotechnology*. Springer, 2012, pp. 457–463.

[22] B. Buchholz, T. J. Armstrong, and S. A. Goldstein, "Anthropometric data for describing the kinematics of the human hand," *Ergonomics*, vol. 35, no. 3, pp. 261–273, 1992.

[23] G. P. Kontoudis, M. V. Liarokapis, A. G. Zisimatos, C. I. Mavrogiannis, and K. J. Kyriakopoulos, "Open-source, anthropomorphic, underactuated robot hands with a selectively lockable differential mechanism: Towards affordable prostheses," in *IEEE/RSJ International Conference on Intelligent Robots and Systems*, 2015, pp. 5857–5862.

[24] R. R. Ma, J. T. Belter, and A. M. Dollar, "Hybrid deposition manufacturing: Design strategies for multimaterial mechanisms via three-dimensional printing and material deposition," *Journal of Mechanisms and Robotics*, vol. 7, no. 2, p. 021002, 2015.

[25] J. Falco, K. Van Wyk, S. Liu, and S. Carpin, "Grasping the performance: Facilitating replicable performance measures via benchmarking and standardized methodologies," *IEEE Robotics & Automation Magazine*, vol. 22, no. 4, pp. 125–136, 2015.